HHS Public Access

Author manuscript

IEEE Trans Biomed Eng. Author manuscript; available in PMC 2015 April 15.

Published in final edited form as:

IEEE Trans Biomed Eng. 2010 December ; 57(12): 2861–2869. doi:10.1109/TBME.2010.2052255.

Reversible Projection Technique for Colon Unfolding

Jianhua Yao, **Ananda S. Chowdhury**[1], **Javed Aman**[1], and **Ronald M. Summers**[1]

[1]Radiology and Image Sciences Department, Clinical Center, the National Institutes of Health, Bethesda, MD, 20892, USA

Abstract

Colon unfolding provides an efficient way to navigate the colon in CT colonography. Most existing unfolding techniques only computed forward projections. When radiologists find abnormalities or conduct measurements on the unfolded view (which is often quicker and easier), it is difficult to locate the corresponding region on the 3D view for further examination (which is more accurate and reliable). To address this, we propose a reversible projection technique for colon unfolding. The method makes use of advanced algorithms including rotation-minimizing frames, recursive ring sets, mesh skinning and cylindrical projection. Both forward and reverse transformations are computed for points on the colon surface. Therefore, it allows for detecting and measuring polyps on the unfolded view and mapping them back to the 3D surface. We generated realistic colon simulation incorporating most colon characteristics such as curved centerline, variable distention, haustral folds, teniae coli and colonic polyps. Our method was tested on both the simulated data and 110 clinical CT colonography data. Comparison of polyp size measurements on the unfolded view and the 3D view clearly demonstrates the importance of our reversible projection technique.

Keywords

CT colonography; unfolding; mesh skinning; reversible projection

1 Introduction

The colon is a convoluted tubular structure. The traditional way to navigate a colon surface along its centerline is not efficient due to the limited view angle and furthermore polyps behind the haustral folds often get obstructed. A more efficient way is to open and unfold the colon and view the surface from above. Although this is not possible in optical colonoscopy, it can be implemented in CT colonography (CTC) via computer graphics techniques. Several investigations [1-3] had showed that colon unfolding could increase the field of view and improve the sensitivity of polyp detection.

Many techniques have been proposed to unfold the colon. They can be put in three categories. The first category is based on raycasting [4]. Vilanova *et al*. [5] unfolded the colon locally using a local projection and then globally mapped the colon using a suitable parameterization. Wang *et al*. [6] proposed a technique using the electrical field of a charged centerline to transform the colon into a straight cylinder-like shape and uniformly sample the planar cross sections orthogonal to the centerline. They then applied a raytracing technique to generate the unfolded view. Sudarsky *et al*. [7] presented an efficient method based on

skeletal subspace deformation and uniform raycasting orthogonal to the central path. The colon unfolding is conducted in two steps. First the colon is straightened using mesh skinning based on the centerline, then the dissection is computed using the ray-casting technique. However, as some papers in this category [7] pointed out, it was difficult to choose the right sampling rate in raycasting-based techniques and structures behind the first object encountered by the rays may be obstructed. The second category is based on conformal texture mapping [8]. Haker *et al*. [9] used an angle-preserving conformal mapping to map the entire colon surface onto a flat plane. Hong *et al*. [10] proposed a conformal mapping based on minimizing harmonic energy to achieve angle preserving and minimum distortion. The 3D surface was mapped to a 2D rectangular map. Huang *et al*. [11] adopted similar conformal mapping approach in their effort to visualize teniae coli on the unfolded view. They demonstrated that the three teniae coli are parallel and evenly distributed. This observation can not be easily appreciated on the original 3D colon view. The techniques in this category have to deal with texture distortion and surface parameterization. They often require high quality surfaces and are computationally expensive. The third category is based on local projection. Paik *et al*. [2] proposed various map projection techniques including cylindrical and planar projection for the fly-through of virtual colonoscopy. They increased the view angle up to 360 degree. In some sense, their technique essentially computed a local unfolded view. Vos *et al*. [12] projected six orthogonal images onto an unfolded cube to render the complete field of view. This was also a local unfolding but introduced extra distortion. Hoppe *et al*. [13] proposed a virtual colon dissection by placing a virtual camera oriented perpendicular to the centerline. The camera displays the inner colon surface with 90° field of view and rotates in 45° increments around the centerline. This technique has trouble seeing polyps behind a fold, and moreover different view panels stitched together create discontinuity.

All the above mentioned colon unfolding techniques only supported forward mapping. That is, only the projection from 3D colon surface to 2D unfolded plane is provided, not the reverse one. In the raycasting based techniques, multiple points may lay in the path of the same casting ray, which causes ambiguity in the reverse projection. In the conformal mapping technique, the reverse transformation is extremely difficult or not available due to the complex transformation. Projection based techniques are the only feasible ones supporting reverse mapping. Without the reverse mapping, when radiologists find abnormalities or conduct measurement on the unfolded view (which is often quicker and easier than on the 3D view), it is difficult to locate the corresponding region in the 3D view for further confirmation and examination (which is more accurate and reliable). To address this problem, we propose a reversible projection technique for efficient colon unfolding. The novelty of our technique and the main contributions are: 1) a recursive ring set method to resolve the centerline and surface correspondence problem (section 2.2); 2) reverse transformation from the unfolded view to the 3D view (section 2.4), and 3) validate the technique using realistic colon simulation and polyp measurement on clinical CTC data (section 2.5).

2 Methods

Our method is summarized as follows. Given a CT colonography data set, the 3D colon surface is first segmented using thresholding, region growing and level sets [14]. Then the centerline of the colon is extracted based on fast marching level set and topographical thinning [15]. Then rotation-minimizing frames (RMF) are established along the centerline. After that, a recursive ring set technique is applied to map vertices on the colon surface to their corresponding centerline points. Next, mesh skinning is employed to straighten the colon. After that, cylindrical projection is applied to unfold the colon. Finally, reverse transformation is computed for every vertex. The flow chart is illustrated in Figure 1.

2.1 Rotation-minimizing frame (RMF)

The colon centerline is a 3D spatial curve in the center of the colon. The centerline is represented as a sequence of 3D points from rectum to cecum. We first fit a 5th degree B-spline curve to the centerline. The B-spline curve utilizes the original centerline as control points and has explicit forms to compute tangent, normal and binormal for every point along the curve [16]. We then discretize the centerline at 0.5 mm resolution (which is approximately the same resolution as the CT data set). The Frenet-Serret frame (FSF) is a common tool to study the differential geometry of spatial curves [17]. The FSF of a given curve $c(u)$ is defined by the tangent $\vec{t}(u)$, normal $\vec{n}(u)$ and binormal $\vec{b}(u)$ vectors of the curve,

$$\vec{t}(u)=\frac{\dot{c}(u)}{\|\dot{c}(u)\|},\ \vec{b}(u)=\frac{\dot{c}(u)\times\ddot{c}(u)}{\|\dot{c}(u)\times\ddot{c}(u)\|},\ \vec{n}(u)=\vec{b}(u)\times\vec{t}(u) \quad (1)$$

here $c(u)$ is one point on the curve, $\dot{c}(u)$ is the first degree derivative and $\ddot{c}(u)$ is the second degree derivative. However, the FSF is not the best choice for our application since it may exhibit strong rotation around the tangent vector. A so-called rotation-minimizing frame (RMF) is more appropriate [17]. The RMF is formed by the tangent vector $\vec{t}(u)$ and two unit vectors $\vec{f}_1(u)$ and $\vec{f}_2(u)$spanning the normal plane at $c(u)$. $\vec{f}_1(u)$ and $\vec{f}_2(u)$ rotate as little as possible around $\vec{t}(u)$ between neighboring frames. They can be derived from the FSF,

$$\begin{aligned}\vec{f}_1(u)&=\sin\Omega(u)\,\vec{b}(u)+\cos\Omega(u)\,\vec{n}(u)\\ \vec{f}_2(u)&=\cos\Omega(u)\,\vec{b}(u)-\sin\Omega(u)\,\vec{n}(u)\end{aligned} \quad (2)$$

here Ω is the angle difference of two neighboring frames,

$$\Omega(u)=-\int_0^u\tau(t)\|\dot{c}(t)\|dt \quad (3)$$

here $\tau=\det\{\dot{c},c,\ddot{c}\}/\|\dot{c}\times c\|^2$ is the torsion of the curve. The proof that the RMF $M(u)=\{\vec{t}(u), \vec{f}_1(u), \vec{f}_2(u)\}$ is rotation-minimizing along the centerline can be found in [17]. Figure 2 illustrates the FSF and RMF of one centerline. In the following description, we use c_j to represent the j^{th} point on the centerline and M_j as its RMF.

2.2 Recursive ring sets

Once the RMF is established, every vertex on the colon surface is associated to its corresponding centerline point and a local RMF. The methods in [5, 7] rely on distance map for this purpose. A distance map stores the distances of vertices to their nearest centerline points and is often computed by Euclidean distance transformation [18]. However, in 3D colon the distance map approach may fail to find the right correspondence in highly curved regions. For instance, in Figure 3a, c_1 is the topological corresponding centerline point of v_1. However, c_2 is closer to v_1 than c_1 in terms of Euclidean distance. Since c_1 and c_2 have different RMFs, the mis-correspondence will cause incorrect transformation in the unfolding process. To resolve this problem, we propose a recursive ring set technique that can establish a topology-preserving correspondence. The concept of ring set was also adopted in the centerline computation in [19], where two parallel planes perpendicular to the local centerline segment were used to generate the a ring set. However, the method in [19] is computational expensive since each vertex needs to be tested for all ring sets. We propose a ring set technique based on recursive refinement to obtain topology-preserving correspondence between the colon surface and its centerline.

The recursive ring set technique is summarized as follows. It is a four-step procedure. In the first step, for every surface vertex v_i, the closest centerline point c_j based on Euclidean distance is recorded as its initial corresponding centerline point, i.e.

$$CL(v_i)=\arg\min_{c_j}(\|v_i - c_j\|) \quad (4)$$

here $CL(v_i)$ represents the corresponding centerline point for v_i. A BSP (binary space partition) tree [20] of the centerline is created to accelerate the searching. The searching time is therefore reduced from O(N) to O(log$N$), where N is the number of points on the centerline.

In the second step, a ring set R_j is created for each centerline point c_j. The initial set for R_j includes all vertices $\{v_i\}$ whose closest centerline point is c_j, i.e.,

$$\forall v_i, if\ CL(v_i)=c_j, then\ v_i \in R_j, \quad (5)$$

In the third step, the ring sets are recursively updated along the centerline. A connected component analysis is conducted for each ring set R_j. Two vertices are considered connected if there is an edge joining them. The largest connected surface patch remains in the ring set, and the rest are removed from R_j and put in a refinement set Q.

In the fourth step, for every point v_k in set Q, its closest neighbor v_m not in set Q is retrieved, i.e.,

$$v_m=\arg\min_{v_m, v_m \notin Q}(\|v_k - v_m\|) \quad (6)$$

and v_m′s corresponding centerline point is assigned to v_k, i.e. $CL(v_k)=CL(v_m)$. The process is repeated until Q is empty. Step 3 and 4 are repeated until there is only one ring set for every centerline point.

The scheme is illustrated in Figure 3a. Here v_1 is in the ring set of c_1, so $CL(v_1)=c_1$. Figure 3b shows the recursive ring sets associated with the centerline (each color strip indicates one ring set).

2.3 Mesh skinning

Mesh skinning [21] is a skeleton-driven deformation technique widely used in computer animation. We apply this technique to straighten the colon using its centerline as the skeleton and the colon surface as the skin. Here we use a similar technique as the one in [7].

This is a two-step procedure. In the first step, the centerline is deformed to form a straight line along the z axis. The straightened centerline is represented as,

$$\begin{aligned} c_j'.x &= c_j'.y = 0 \\ c_j'.z &= c_{j-1}'.z + \|c_j - c_{j-1}\| \end{aligned} \quad (7)$$

here c_j and c_j' are the coordinates in the original and straightened centerlines respectively. In the second step, the vertices on the colon surface are transformed using the RMF associated with their corresponding centerline point $CL(v_i)$. The transformation is written as,

$$v_i' = c_j' + M_j^{-1}(v_i - c_j) \quad (8)$$

here $c_j = CL(v_i)$ is the corresponding centerline point of v_i, M_j is the RMF of c_j. In order to achieve a smooth transformation, we adopt the strategy in [7] to include a neighborhood of c_j in the calculation. The new transformation is then updated as,

$$v_i' = \sum_{k=j-\delta}^{k=j+\delta} w_{i,k}\left(C_k' + M_k^{-1}(v_i - c_k)\right) \quad (9)$$

here δ is the neighborhood range (default value is 3), $w_{i,k}$ is the weight which is defined to be inversely proportional to the distances $d_{i,k}$ between vertex v_i and centerline point c_k, i.e.,

$$\begin{aligned} w_{i,k} &= \frac{d_{i,k}^{-1}}{\sum_{j=k-\delta}^{j=k+\delta} d_{i,k}^{-1}} \\ d_{i,k} &= \|v_i - c_k\| \end{aligned} \quad (10)$$

Figure 4 shows the straightened colon using mesh skinning and one close-up view.

2.4 Reversible projection and colon unfolding

Cylindrical projection is widely used in geographical map projection to unfold the earth onto a 2D map [22]. In the cylindrical map projection, the meridians are mapped to equally-spaced vertical lines and circles of latitude are mapped to horizontal lines. One trait of cylindrical projection is its ability to preserve distance on the surface. Similarly, we can unfold the straightened colon using the cylindrical projection. In analogy to geographic map, the colon centerline is the analogue of the Earth's axis of rotation.

The cylindrical projection maps every point on the straightened colon onto a plane at y=0. We preserve the distance-to-centerline function for every vertex by mapping it as the height elevation above the plane. The projection and unfolding are written as,

$$\begin{aligned}\tilde{\nu}_i.z &= \nu_i'.z \\ \tilde{\nu}_i.y &= \sqrt{(\nu_i'.x)^2+(\nu_i'.y)^2} \\ \tilde{\nu}_i.x &= \arctan(\nu_i'.y, \nu_i'.x) \times \tilde{\nu}_i.y\end{aligned} \quad (11)$$

here $\tilde{\nu}_i$ is the coordinate of vertex ν_i on the unfolded colon, $\tilde{\nu}_i.z$ is the distance along the centerline, $\tilde{\nu}_i.y$ is the distance to the centerline, and $\tilde{\nu}_i.x$ is the arc length around the centerline. We cut open the colon at 0° meridian when unfolding the colon. An edge (ν_i, ν_j) is removed from the unfolded colon if it is across 0° meridian, i.e. arctan($\nu_i'.y$, $\nu_i'.x$)*arctan($\nu_j'.y$, $\nu_j'.x$)<0. All other edges are retained. Therefore the unfolded colon is essentially a 3D surface. Since there is one-to-one correspondence between the 3D colon and the unfolded one, we not only preserve the topology of the original colon surface but also the vertex resolution. Figure 5 shows the unfolded colon and two close-up views. Our method can handle totally collapsed colon segments.

Furthermore, the projection from the 3D colon to the unfolded colon is reversible. The reverse projection of Eq. 11 can be computed in two steps (Eq. 12 and Eq. 13). Given a coordinate $\tilde{\nu}_i$ in the unfolded colon, the coordinate in the straightened colon ν_i' can be obtained as,

$$\begin{aligned}\nu_i'.x &= \tilde{\nu}_i.y \times \cos\left(\frac{\tilde{\nu}_i.x}{\tilde{\nu}_i.y}\right) \\ \nu_i'.y &= \tilde{\nu}_i.y \times \sin\left(\frac{\tilde{\nu}_i.x}{\tilde{\nu}_i.y}\right) \\ \nu_i'.z &= \tilde{\nu}_i.z\end{aligned} \quad (12)$$

We can further compute the reverse transformation from the straightened colon to the original 3D colon using the following equation,

$$\nu_i = c_j + M_j(\nu_i' - c_j') \quad (13)$$

Combining (12) and (13), a point $\tilde{\nu}_i$ on the unfolded colon can be reversely projected back to a point ν_i on the original 3D colon. The reverse transformation allows a user to locate and measure lesions on the unfolded colon and then map them back to the 3D colon for

confirmation. This provides an easier and quicker way than performing the measurement task directly on the 3D colon.

2.5 Algorithm complexity

Our technique is computational efficient. We conduct a complexity analysis by breaking down to the three main parts of the algorithm: recursive ring sets, mesh skinning and reversible projection.

In the following analysis, N is the number of centerline points and V is the number of colon vertices. V is much greater than N in our analysis.

In the recursive ring sets stage, step 1 requires every colon vertex to search for its closest centerline point, the time complexity is O(V log$N$). Step 2 needs to locate the ring set for every vertex (O(V)). Step 3 involves connected component analysis for every ring set. The complexity is O(N * K log$K$), where K is the average number of vertices in a ring set and K=V/N. Therefore the complexity in step 3 can be further simplified as O(V log (V/N)). Step 4 is the rearrangement of vertices in set Q, the complexity is O(Q), where $Q \ll V$. Therefore is the complexity for the recursive ring set is O(V log$N$)+O(V)+O(V log(V/N)+O(Q) = O(V log$N$).

In the mesh skinning stage, step 1 is the straighten of the colon centerline, the complexity is O(N). Step 2 is the mesh skinning of colon vertices, the complexity is O(V). The complexity for mesh skinning is then O(N)+O(V)=O(V).

In reversible projection stage, every vertex on the colon is projected to a flat plane. The complexity is O(V).

Therefore, the overall complexity of the entire algorithm is

$$\mathrm{O}(V\log N)+\mathrm{O}(V)+\mathrm{O}(\nu)\mathrm{VO}(V\log N) \quad (14)$$

2.6 Colon simulation and CTC data

Our colon unfolding technique is evaluated using both simulated colon data and clinical CTC data.

We created a realistic colon simulation using the mesh skinning technique in three steps. First, a digital phantom of a cylindrical tube model with haustral folds and teniae coli is built (Figure 6a). Haustral folds are added in the form of indentations onto the tube. The folds are modeled as a series of trisected torus with elliptic cross-sections. The trisections are partitioned equally in circumferential location at 0, 120 and 240 degrees on the cross-section plane on the digital phantom. The spaces between the trisection are in accordance with the appearance of teniae coli. Second, the centerline from a clinical CTC is computed and employed. Every point on the centerline is equipped with a rotation-minimizing frame (Section 2.1) and its associated distention value computed from the CTC data. Third, mesh skinning (Section 2.3) is applied to warp the tube phantom around the centerline and

generate realistic colon simulation. Simulation of colonic polyps, modeled as semi-ellipsoids, can also be added to the phantom. Figure 6b shows the surface of the colon simulation. Figure 6c shows the surface of a real colon whose centerline and distention data is employed to generate the simulation in Figure 6b. The simulated colon highly resembles the real one. To our best knowledge, this is the first colon simulation that incorporates most colon characteristics in one model, including curved centerline, variable distention, haustral folds, teniae coli and colonic polyps.

The clinical CTC data are acquired in three institutions. Each patient was scanned in both supine and prone positions. CT scanning parameters included 1.25- to 2.5-mm section collimation and 1-mm reconstruction interval. Each data set has more than 400 slices on average. To evaluate the quality of the unfolded colon, an expert visually examined every case. An unfolded colon is judged as satisfactory if the colon features such as haustral folds and polyps are preserved and can be easily identified. We also recorded the computation time for the unfolding process.

2.7 Polyp size measurement on unfolded colon

Estimating the size of a polyp is essential in CTC diagnosis since large polyps are more likely to become malignant and cancerous. To explore the reverse transformation brought by our technique, we conduct and compare the polyp measurement on both the 3D view and the unfolded view. Here the polyp size is defined as the largest diameter across the polyp determined by the operator. In this experiment, the operator first conducted the measurement on the unfolded surface and recorded the two endpoints. The two endpoints were then mapped to the 3D surface for additional measurement. Figure 7 illustrates a polyp on both the 3D view and the unfolded view.

3 Results

We ran tests on the simulated colon to validate the capability of our unfolding technique in preserving the location, orientation and size information. Haustral folds were used as the landmarks. Figure 8 shows the unfolded view of the colon simulation and the ground truth of the unfolded view. We located the two endpoints of the middle folds on both the unfolded view and the ground truth view. We then compared the difference of the fold location (midpoint of two endpoints), orientation (direction of two endpoints) and size (distance between two endpoints). Table 1 summarizes the statistics of the comparison for 49 folds. We were able to achieve sub-voxel accuracy (voxel size is $1mm^3$)

Our method was then tested on 110 clinical CTC studies. All unfolded colons were determined visually acceptable. The average computation time on a 3.0 GHz Pentium processor with 4GB RAM was 14.9 ± 3.8 seconds. Currently our algorithm is not optimized for speed. Figure 5 shows one example of the unfolded colon. Our method succeeded in unfolding the collapsed section near the rectum.

We conducted dimensional measurements for 103 colonic polyps on both the 3D colon surface and the unfolded surface. Figure 9 shows the scatter plot of the two sets of measurements on the 3D vs. unfolded views. The two measurements show high-degree

correlation. The equation for the linear regression is $y=1.07x$, which indicates the unfolded view tends to give larger measurements when the colon is straightened. Our reversible projection provides an efficient and reliable polyp measurement tool. The operator can conduct the measurement on the unfolded view (which is often quicker and easier to do), and then reversely project the endpoints to the 3D view for verification and generation of the 3D measurement.

4 Discussion and Conclusion

Both our method and the one described in [7] used the mesh skinning technique to straighten the colon and were much more efficient than other prevalent methods. However, our method shows several improvements over the one discussed in [7]. First and foremost, we developed a novel recursive ring set technique to find the topology-preserving correspondence between the centerline and vertices on the colon surface. It is more robust and does not rely on the distance map computed from the original CT data. Secondly, we do not use raycasting. We use a cylindrical projection instead to map the vertices to the rotation-minimizing frames along the centerline so that it preserves the resolution and topology of the 3D surface and avoids the obstruction problem. Thirdly, our method supports reverse transformation from the unfolded colon to the original 3D colon, which allows us to conduct the polyp measurement and detection on the unfolded view. Finally, our technique maps each vertex onto the unfolded plane instead of sampling the centerline and surface, so that we can avoid the undersampling (missing polyps) and oversampling (double polyps) problems that occur in some other methods [5]. Though Paik *et al*. [2] adopted a similar cylindrical projection in their virtual colon fly-through to increase the view angle; the technique was limited to the local view field and their projection was not reversible.

In conclusion, we presented a computationally efficient reversible projection technique for colon unfolding based on recursive ring set formulation, mesh skinning and cylindrical projection. The above techniques have their origins in diverse areas like computer animation and geographical mapping. The proposed method is quite robust and works for all colon segments including poorly distended ones. The method has been tested on realistic colon simulation and 110 clinical data sets. It achieved sub-millimeter level accuracy in the simulation data and generated satisfying results in the clinical data. The technique supports polyp measurement on the unfolded view, an essential feature for virtual colonoscopy.

In the future work, we are investigating effective ways to integrate our technique in colon navigation and computer aided detection. We also plan to apply the realistic colon simulation in other research areas, such as supine and prone colon registration, tenia coli detection and colon segmentation.

Acknowledgments

The authors thank Perry J. Pickhardt, William R. Schindler and Richard Choi for providing computed tomographic colonography and supporting data. This research was supported by the Intramural Research Program of the National Institutes of Health, Clinical Center.

References

1. Johnson KT, et al. CT colonography using 360-degree virtual dissection: a feasibility study. AJR Am J Roentgen. 2006; 186:90–95.
2. Paik DS, et al. Visualization modes for CT colonography using Cylindrical and Planar Map Projections. Journal of Computer Assisted Tomography. 2000; 24(2):179–188. [PubMed: 10752876]
3. Silva AC, Wellnitz CV, Hara AK. Three-dimensional Virtual Dissection at CT Colonography: Unraveling the Colon to Search for Lesions. Radiographics. 2006; 26:1669–1686. [PubMed: 17102043]
4. Ray H, et al. Ray casting architectures for volume visualization. IEEE Transaction on Visualization and Computer Graphics. 1999; 5(3):210–222.
5. Vilanova, A.; Groller, E. Geometric Modeling for Virtual Colon Unfolding. In: Brunnett, G., et al., editors. Geometric Modeling for Scientific Visualization. Birkhauser; 2004. p. 488
6. Wang G, et al. GI tract unraveling with curved cross sections. IEEE Trans Med Imag. 1998; 17(2): 318–322.
7. Sudarsky, S., et al. MICCAI. New York: Springer-Verlag Berlin Heidelberg; 2008. Colon Unfolding Via Skeletal Subspace Deformation.
8. Haker S, et al. Conformal Surface Parameterization for Texture Mapping. IEEE Transaction on Visualization and Computer Graphics. 2000; 6(2):181–189.
9. Haker S, et al. Nondistorting flattening maps and the 3-D visualization of colon CT images. IEEE Trans Med Imag. 2000; 19(7):665–670.
10. Hong W, et al. Conformal Virtual Colon Flattening. SPM. 2006:85–93.
11. Huang, A.; Roy, D.; Summers, RM. IEEE Visualization. Baltimore, MD: 2005. Teniae coli guided navigation and registration for virtual colonoscopy.
12. Vos, FM., et al. MICCAI. Springer; Heidelberg: 2001. A New Visualization Method for Virtual Colonoscopy.
13. Hoppe H, et al. Virtual Colon Dissection with CT Colonography Compared with Axial Interpretation and Conventional Colonoscopy: Preliminary Results. AJR Am J Roentgen. 2004; 182:1151–1158.
14. Franaszek M, et al. Hybrid segmentation of colon filled with air and opacified fluid for CT colonography. IEEE Trans Med Imag. 2006; 25(3):358–368.
15. Van Uitert RL, Summers RM. Automatic correction of level set based subvoxel precise centerlines for virtual colonoscopy using the colon outer wall. IEEE Trans Med Imag. 2007; 26(8):1069–78.
16. Weisstein, EW. CRC Concise Encyclopedia of Mathematics. Second. Chapman & Hall/CRC; 1999.
17. Maurer C, Juttler B. Rational approximation of rotation minimizing frames using Pythagorean-hodograph cubics. Journal for Geometry and Graphics. 1999; 3(2):141–159.
18. Cuisenaire O, Macq B. Fast Euclidean Distance Transformation by Propagation Using Multiple Neighborhoods. Comput Vis Image Understanding. 1999; 76(2):163–172.
19. Iodanescu G, Summers RM. Automated centerline for computed tomography colonography. Academic Radiology. 2003; 10:1291–1301. [PubMed: 14626304]
20. Fuchs H, Kedem ZM, Naylor BF. On visible surface generation by a priori tree structures. SIGGRAPH. 1980; 14(3):124–133.
21. Lewis JP, Cordner M, Fong N. Pose Space Deformation: A Unified Approach to Shape Interpolation and Skeleton-Driven Deformation. proceeding of ACM SIGGRAPG. 2000:165–172.
22. Snyder, JP. Map Projections - A Working Manual. USGS; 1987.

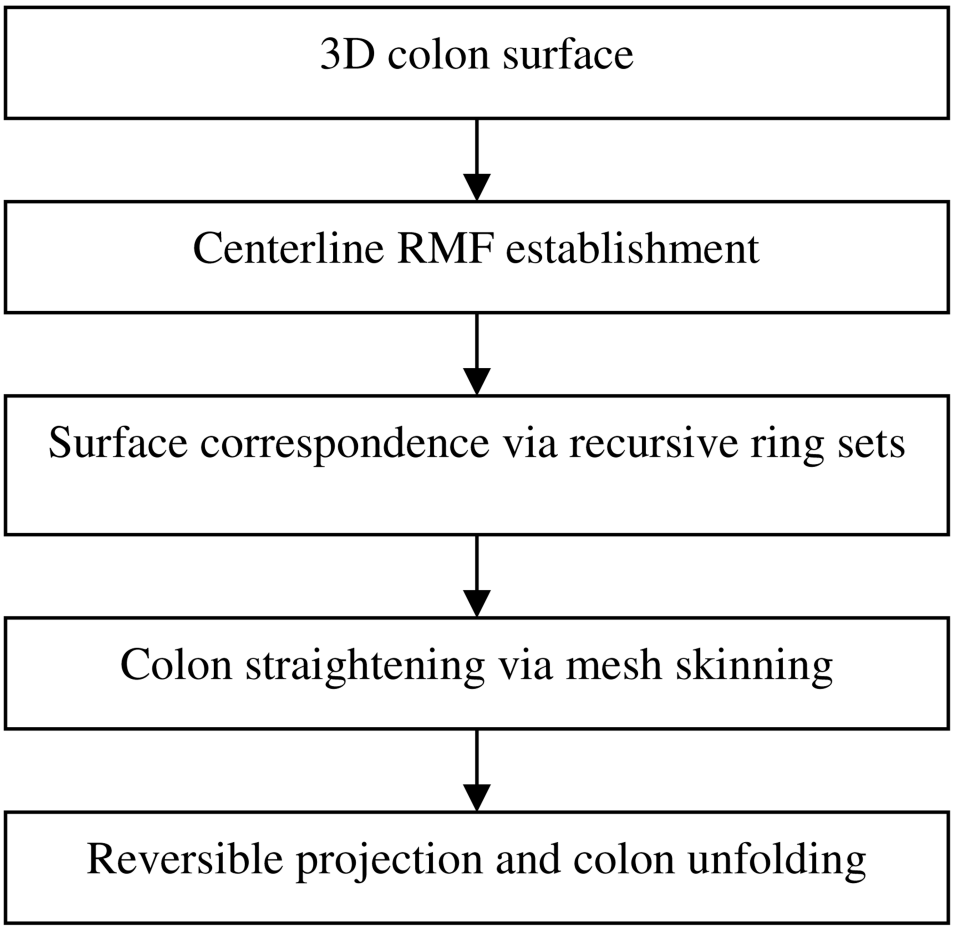

Figure 1. Method overview

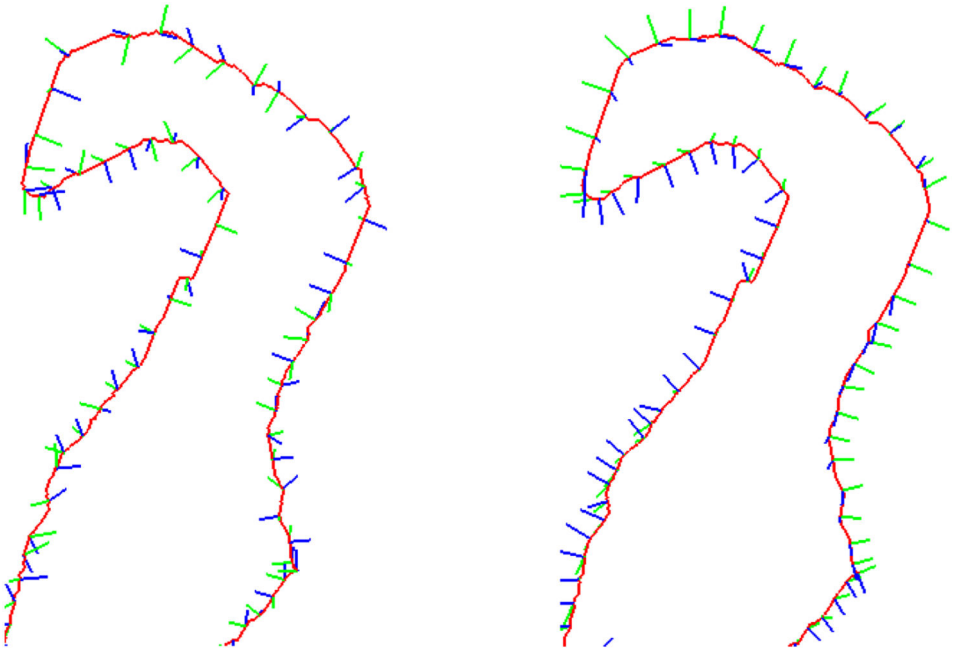

Figure 2. Frenet-Serret frame (FSF) and rotation-minimizing frame (RMF)
Left: FSF, blue: $b(\vec{u})$, green: $n(\vec{u})$
Right: RMF, blue: $f_1(\vec{u})$, green: $f_2(\vec{u})$

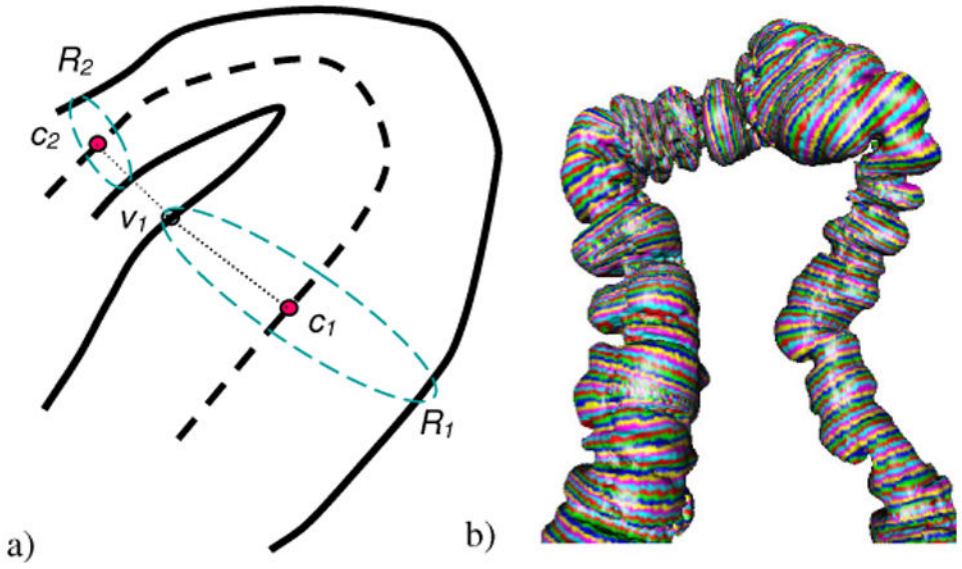

Figure 3. Recursive ring sets

a) Method scheme (solid line: colon wall, thick dashed line: centerline, thin dashed line: ring sets), b) ring sets associated with the centerline (color strips).

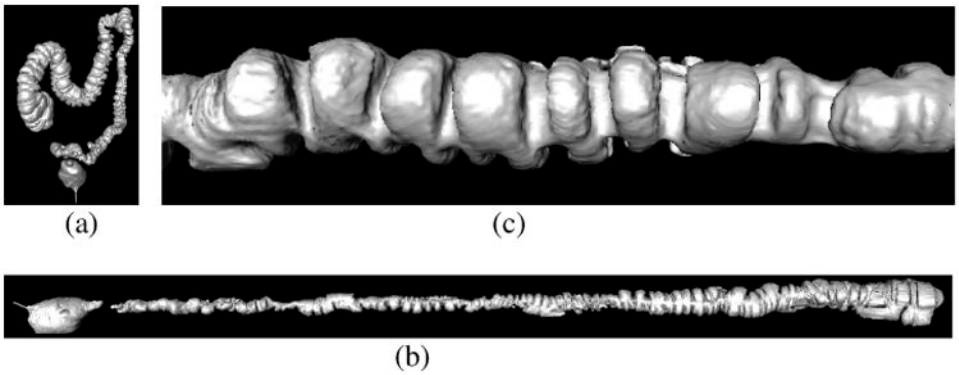

Figure 4. Colon straightening using mesh skinning

a) Original 3D colon, b) straightened colon, c) close-up view of the straightened colon.

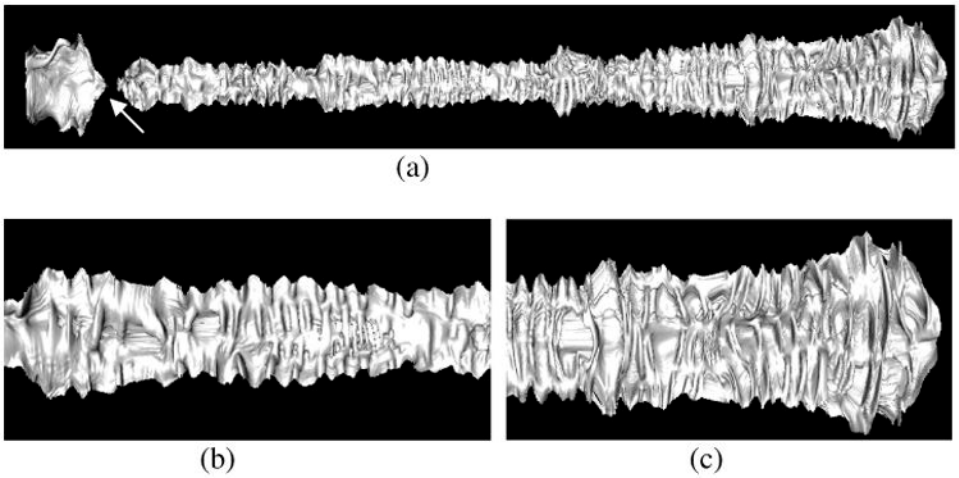

Figure 5. Unfolded colon

a) Entire unfolded colon, b,c) close-up views. One section near the rectum is collapsed (arrow).

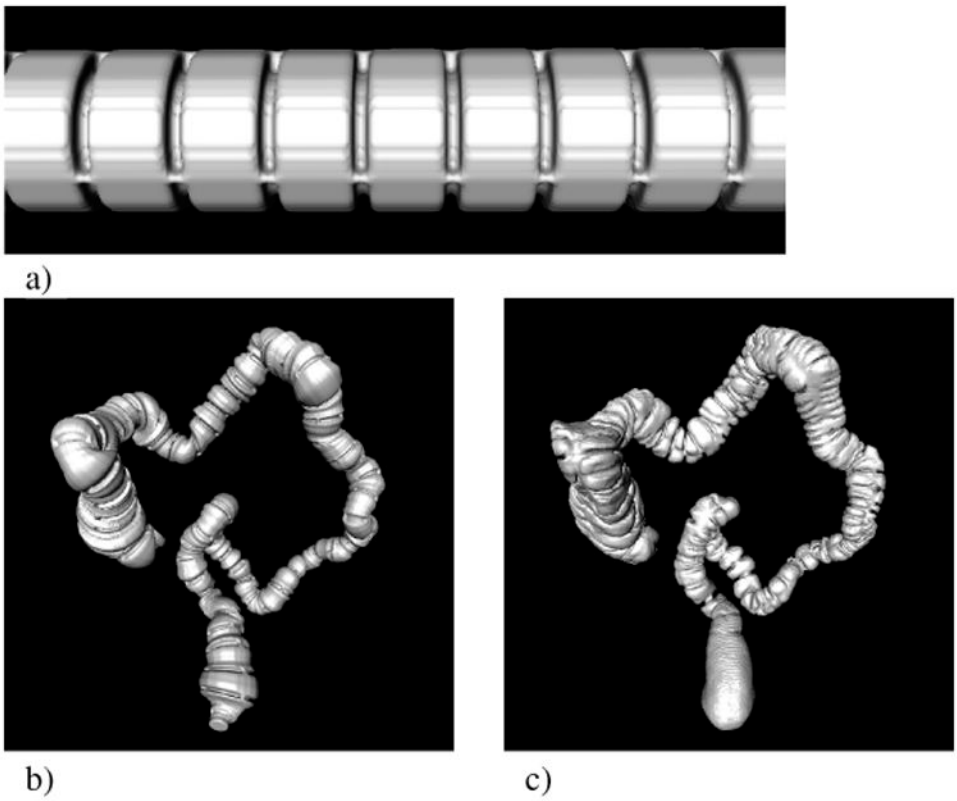

Figure 6. Colon simulation

a) digital phantom of a cylindrical tube with haustral folds and teniae coli, b) surface of a simulated colon, c) surface of a real colon whose centerline and distention are used in b).

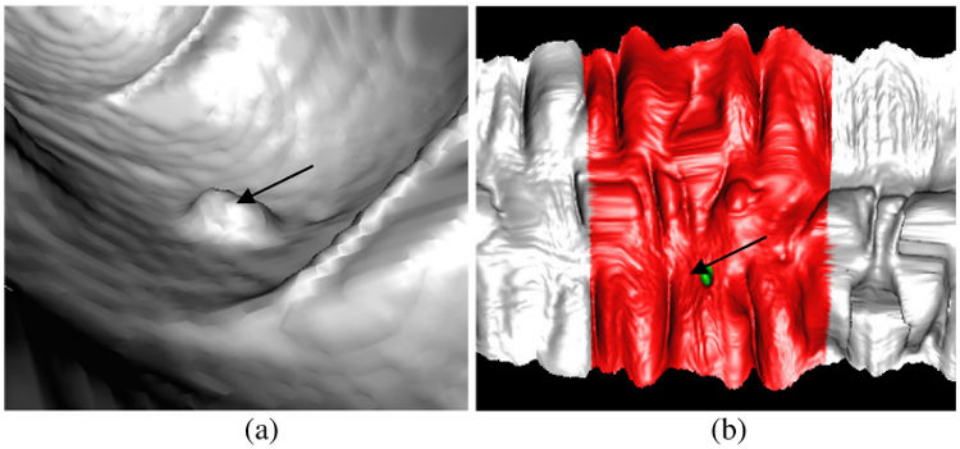

Figure 7. Polyps in 3D and unfolded view

a) 3d view, b) unfolded view, Green: polyp, red: a neighborhood

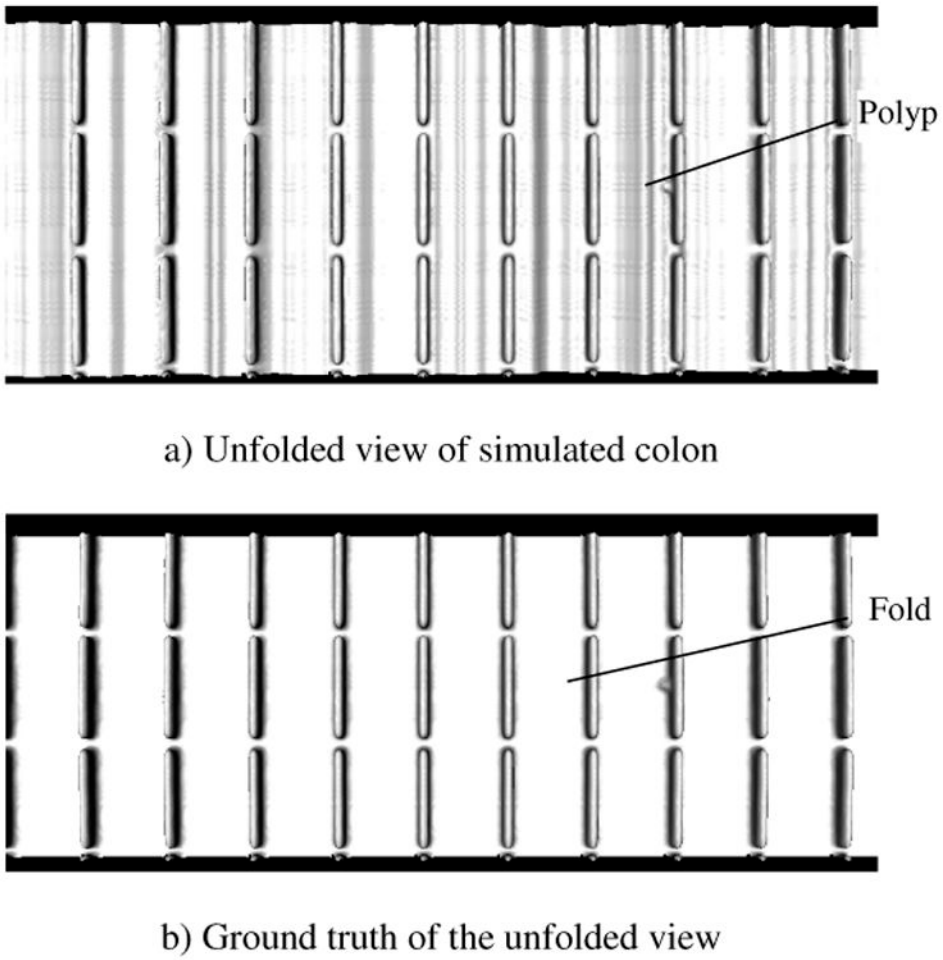

Figure 8. Unfolded view of simulated colon and ground truth

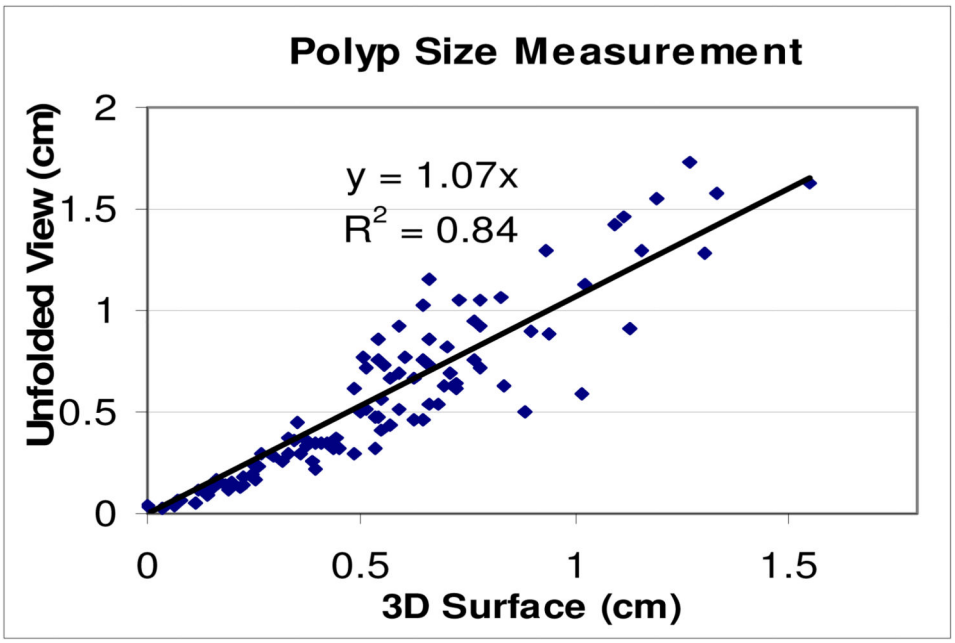

Figure 9. Polyp size measurement on 3D surface and unfolded view

Table 1

Fold comparison between unfolded view (UV) and ground truth (GT) for the simulated colons (N=49)

|UV-GT|	Location	Orientation	Length
Mean	0.42 mm	0.45°	0.43 mm
Stdev	0.29 mm	0.47°	0.07 mm